

An Efficient Nanocatalyst Cobalt Copper Zinc Ferrite for the Thermolysis of Ammonium Nitrate

Pragnesh N Dave* and Ruksana Sirach

Cite This: *ACS Omega* 2022, 7, 43784–43792

Read Online

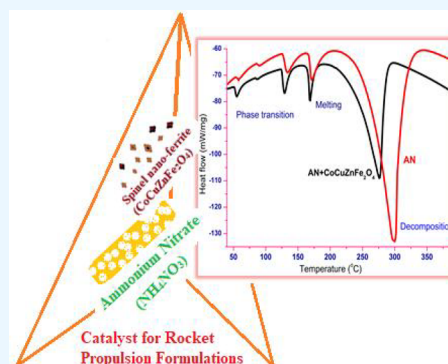
ACCESS |

Metrics & More

Article Recommendations

Supporting Information

ABSTRACT: This work reports synthesis and catalytic effect of cobalt copper zinc ferrite ($\text{CoCuZnFe}_2\text{O}_4$) on the thermal decomposition of ammonium nitrate (AN). AN is a crystalline hygroscopic powder widely applicable as an oxidizer in the propellant formulations for high energetic materials but requires improvement in its thermal decomposition characteristics. Nanocatalyst spinel ferrite $\text{CoCuZnFe}_2\text{O}_4$ was prepared using the coprecipitation method and characterized by various physicochemical instrumental techniques like XRD, FE-SEM, UV-vis, Raman, and TG-DSC. Catalytic study of AN in the presence of nano- $\text{CoCuZnFe}_2\text{O}_4$ was investigated using DSC analysis. The Raman and XRD study confirm the formation of ferrite with a crystalline size 9–22 nm. TG suggests that the catalyst was thermally stable up to 400 °C with ~10% mass loss. The UV-vis study shows that the optical band gap energy of $\text{CoCuZnFe}_2\text{O}_4$ was 2.6 eV, which may help in fast acceleration of electrons during thermolysis of AN, making the thermal decomposition of AN more favorable in the presence of $\text{CoCuZnFe}_2\text{O}_4$. The thermal decomposition investigation suggests that the activation energy of AN thermolysis in the presence of 2 wt % $\text{CoCuZnFe}_2\text{O}_4$ was decreased by ~37%. It is concluded that $\text{CoCuZnFe}_2\text{O}_4$ can be used as an efficient catalyst for improving AN's thermal characteristics.



1. INTRODUCTION

Propellant oxidizers are widely used in energetic materials that provide a large amount of oxygen to thrust the device, mainly rockets and missiles for military purposes.^{1–4} Moreover, these oxidizers are organic or inorganic substances, and contain chemical energy that is stored in their propulsion formulation, which produces huge gaseous products with a large amount of heat upon their decomposition process. These highly energetic formulations are used as propellants, pyrotechnics, or explosives.^{5–9} Ammonium nitrate (NH_4NO_3 or AN) based propellants are widely used because of their efficient energetic characteristic.^{10–12}

For energetic purposes, to improve essential properties such as reduction in thermal decomposition temperature, increase thermal decomposition rate, and sensitivity to external stimuli of propellant oxidizers like ammonium perchlorate (AP), 1,3,5,7-tetranitro-1,3,5,7-tetrazocane (HMX), 1,3,5-trinitro-1,3,5-triazine (RDX), nitrotriazolone (NTO), and AN, a nanosized additive or catalysts are added.^{13–15} Investigations in previous studies indicated that in the presence of the nanosize catalyst, the thermal decomposition of AN is enhanced because of the decreased size of the catalyst and the large surface area available for absorption, which enhances the percentage of thermal decomposition of AN.^{16–18} The addition of catalysts like nanometals, nanometal oxides, metal alloys, acids, and organic and inorganic salts on the thermal behavior and thermal safety of AN have been largely investigated.^{19–21} The thermal stability of AN under different

heating rates, gas flow rates, and masses taken during analysis of AN + nanocatalyst is very interesting, and it is an important point to evaluate the studies based on AN thermolysis.^{22,23} Various nanosize ferrites are successfully utilized to improve the thermal decomposition of propellants. Ferrites have a general formula of MFe_2O_4 , where M generally represents metals such as Co^{2+} , Cu^{2+} , Zn^{2+} , etc. Ferrites find applications in a wide range of applications such as gas sensing, photocatalytic degradation, organic synthesis, and magnetic hyperthermia, etc. The ferrites are widely explored for their catalytic effect on the degradation of organic compounds, where the optical band gap of the ferrites widely influences their catalytic efficiency and which is affected by substitution with different metal ions in the ferrite system.^{24–28} Spinel ferrite has two interstitial sites, tetrahedral and octahedral, in its crystal structure, that may support a wide variety of cations, allowing ferrites to have a wide range of characteristics. Other divalent metal ions can be substituted for M, resulting in a variety of spinel ferrites.^{29–31} Previous literature has suggested that Al^{3+} substitution in cobalt ferrite nanoparticles alters the

Received: July 29, 2022

Accepted: October 14, 2022

Published: November 26, 2022



electromagnetic characteristics of CoFe_2O_4 which can be a potential candidate for microwave and power devices applications.³² Substitution of Zn in MgFe_2O_4 increases the resistivity and the magnetic property decreases.³³ The semiconducting behavior of the samples becomes a trend after Cr^{3+} substitution. Substitution of Cr^{3+} ions in the nickel–zinc ferrite system shows increasing resistivity, which allows the prepared samples to be used in higher frequency ranging systems.³⁴ In addition to improving the activation energy and thermal decomposition of propellants, the ferrites are easily separated from the propellants using an external magnet. Many synthetic procedures, such as sol–gel, the hydrothermal method, and the coprecipitation method, etc., are utilized for the synthesis of ferrite nanoparticles.^{20–23,29,30} Among these methods, the coprecipitation method is widely utilized because of its lower energy consumption, generation of fewer hazardous byproducts during the synthesis, simplicity of the method, and ease of availability of raw chemicals.

In the present article, the authors are reporting for the first time the effect of cobalt copper zinc ferrite ($\text{CoCuZnFe}_2\text{O}_4$) on the thermal decomposition of AN. $\text{CoCuZnFe}_2\text{O}_4$ nanoparticles were synthesized using the coprecipitation method and its physicochemical properties were characterized accordingly. The effect of $\text{CoCuZnFe}_2\text{O}_4$ nanocatalyst on the thermal decomposition of ammonium nitrate (AN) was investigated using TG-DSC-DTA thermal treatments, and the data were used for the calculation of the activation energy of AN with and without nanocatalyst $\text{CoCuZnFe}_2\text{O}_4$ using the Arrhenius relation.

2. COBALT COPPER ZINC FERRITE

2.1. Material Design. All the chemicals used were of analytical grade without further purification and available from commercial sources: cobalt(II)nitrate hexahydrate [$\text{Co}(\text{NO}_3)_2 \cdot 6\text{H}_2\text{O}$, 99%], copper(II)nitrate trihydrate [$\text{Cu}(\text{NO}_3)_2 \cdot 3\text{H}_2\text{O}$, 95%], zinc(II)nitrate hexahydrate [$\text{Zn}(\text{NO}_3)_2 \cdot 6\text{H}_2\text{O}$, 99%], ferric(III)nitrate nonahydrate [$\text{Fe}(\text{NO}_3)_3 \cdot 9\text{H}_2\text{O}$, 98%], and sodium hydroxide (NaOH). Laboratory-setup triple distilled water was used as a solvent. Ammonium nitrate (AN) was provided by National Chemicals. General tools for preparation such as magnetic stirrer, volumetric glass wares, filtration unit, oven, and tube furnace were purchased through grant number SR/NM/NT-1014/2016 (G) which was available from the Department of Science and Technology (DST), New Delhi, India.

2.2. Preparation of Nanocatalyst Cobalt Copper Zinc Ferrite. Cobalt copper zinc ferrite powder was synthesized by coprecipitation method^{35–37} in which stoichiometric amounts of the hydrated form of cobalt nitrate, copper nitrate, and ferric nitrate were dissolved in triple distilled water. Into this mixture, 2 M sodium hydroxide solution prepared in triple distilled water was added dropwise and allowed to react with it under vigorous stirring. The mixture was allowed to stir for some time until complete precipitation, and a pH \sim 12 was noted. The product obtained was washed with repeated hot triple distilled water until free from salt impurities, vacuum filtered, then washed with hot water to remove nitrate impurities, dried in an oven at 70 °C, and then calcinated at 350 °C for 4 h. The final product obtained was a crystalline powder of metal spinel ferrite $\text{CoCuZnFe}_2\text{O}_4$ which was further characterized by XRD, UV–visible, Raman, FE-SEM, and TG-DSC analyses. Moreover, its catalytic performance was investigated by applying to ammonium nitrate (AN) to study its effect on

thermal decomposition of ammonium nitrate. For that study, the catalyst ($\text{CoCuZnFe}_2\text{O}_4$) and propellant oxidizer (AN) were mechanically mixed at a mass ratio of 2:98.

2.3. Physico-chemical Measurements. Powder XRD analysis of the spinel ferrite $\text{CoCuZnFe}_2\text{O}_4$ was performed on Ultima-IV X-ray diffractometer at 40 mA and 40 kV in the 2θ range of 10° to 80° using $\text{Cu K}\alpha$ radiation having a wavelength of 1.5406 Å. The obtained pattern was evaluated by Powder-X and X'pert HighScore plus software. Optical properties like absorbance and energy band gap of spinel ferrite $\text{CoCuZnFe}_2\text{O}_4$ were measured on Shimadzu UV-1800, UV (ultraviolet)-visible spectrophotometer and recorded in the range 200 nm –800 nm. The Raman spectra were measured by micro-Raman STR 500 having an excitation source of 532 nm at room temperature and ambient pressure and recorded in the range of 50 cm^{-1} to 1700 cm^{-1} wavenumbers. FE-SEM (field emission scanning electron microscope) was used to determine the morphology of pure AN and spinel ferrite $\text{CoCuZnFe}_2\text{O}_4$ and this was captured on a Nova nano FEG (field emission gun)-SEM 450 equipment. TG-DSC analysis of spinel ferrite $\text{CoCuZnFe}_2\text{O}_4$ was performed on a TA/SDT-2790 using a DSC-60, and thermographs were recorded of the samples in an aluminum pan in inert nitrogen atmosphere in the range of ambient to 800 °C. However, the catalytic study of $\text{CoCuZnFe}_2\text{O}_4$ on the thermolysis of AN was measured on TA, Q600-SDT instrument in which simultaneous TG-DSC-DTA measurements were done in the range of room temperature to 400 °C at 5, 10, and 15 °C/min heating rates.

3. RESULTS AND DISCUSSION

3.1. Diffraction Analysis. A typical XRD pattern of the prepared nanocrystal spinel ferrite $\text{CoCuZnFe}_2\text{O}_4$ is shown in Figure 1 and compared with candidate no. 01-077-0012; the

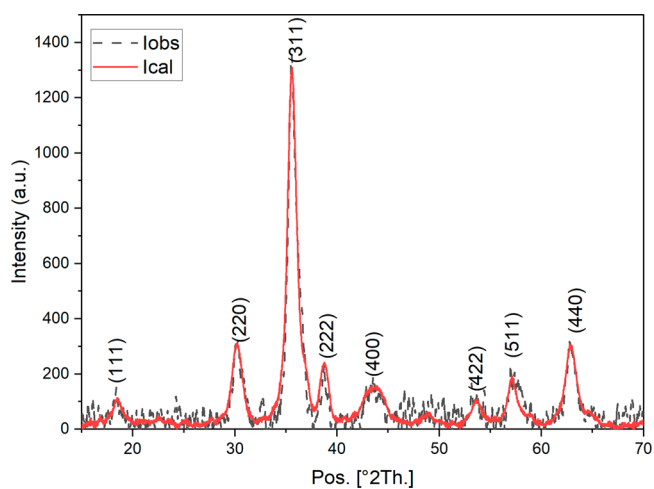


Figure 1. Powder XRD of nanocatalyst $\text{CoCuZnFe}_2\text{O}_4$ (spinel ferrite).

peak indexing is provided in Figure S1 (supplementary file). The $\text{CoCuZnFe}_2\text{O}_4$ has nanoparticles with crystalline size found to vary in the range 9 to 22 nm revealing its degree of crystallinity. This crystalline size was evaluated by Scherrer formula (eq 1).^{38–40} Powder XRD of $\text{CoCuZnFe}_2\text{O}_4$ has peaks at 2θ values of 18.5°, 30.3°, 35.6°, 38.7°, 43.4°, 53.8°, 57.3°, and 62.9° with corresponding lattice planes (111), (220), (311), (222), (400), (422), (511), and (440), respectively.^{41–43} The average crystalline size of CoCuZnF was

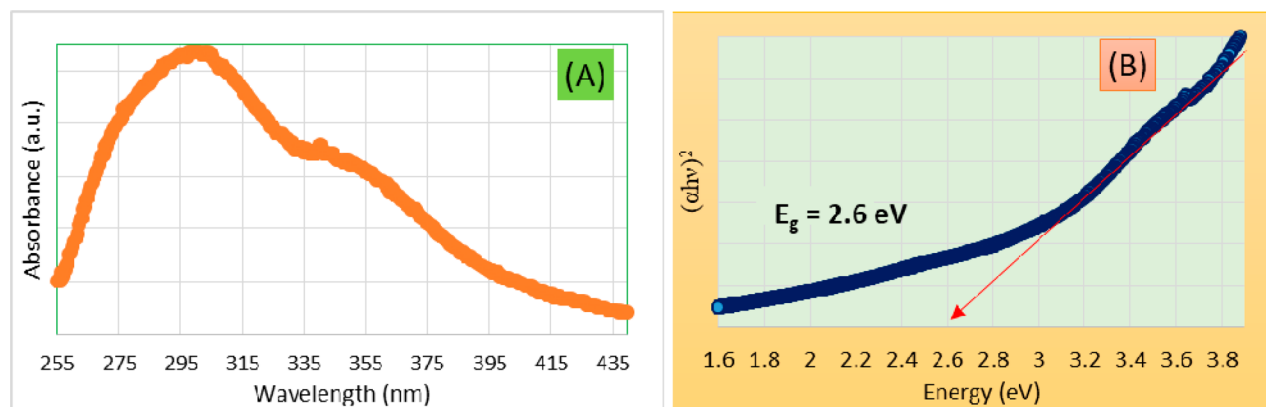


Figure 2. UV-vis spectrum of nano-CoCuZnFe₂O₄: (A) Optical absorbance and (B) Tauc's plot.

13.68 nm, confirming the nanosize of the CoCuZnF particles. Here, spinel ferrite CoCuZnFe₂O₄ synthesized via the coprecipitation method has cubic and cubic crystal symmetry. These forms were confirmed by its lattice parameters such as for the cubic phase, it should have crystal axis $a = b = c$ and crystal angle $\alpha = \beta = \gamma = 90^\circ$, while for the tetragonal phase, it should have crystal axis $a = b \neq c$ and crystal angle $\alpha = \beta = \gamma = 90^\circ$. Unit cell parameters such as lattice constant ($a = b = c$), and X-ray density (X_d) were calculated by using eqs 2 and 3, respectively. Lattice-strain (ϵ) was calculated by using the relation $\epsilon = \beta \cos \theta/4$. Unit cell volume (V) can be given by $V = a^3$. The % porosity (%P) of CoCuZnFe₂O₄ was calculated by $\%P = 1 - (\text{bulk density}/X\text{-ray density}) \times 100$. The dislocation density (δ) was calculated by $\delta = 1/D^2$ lines/m², where D is the crystalline size.

$$D = K \frac{\lambda}{\beta} \cos \theta \quad (1)$$

$$d = \frac{a}{(h^2 + K^2 + l^2)^{1/2}} \quad (2)$$

$$X_d = \frac{8M}{Na^3} \quad (3)$$

where λ is the wavelength of X-ray used (1.5406 Å), D is the crystallite size, K is the crystallite shape factor which is taken as 0.9 in this case considering the particles to be spherical in general. B is full width at half maxima of the XRD peak belonging to 311 plane, a is the lattice parameter (cm) and (hkl) are Miller indices. X_d is X-ray density, d is interplanar spacing, M is molecular weight of sample, and N is Avogadro's number. The cell parameter, lattice strain, X-ray density, cell volume, dislocation density, and porosity of CoCuZnFe₂O₄ was found to be 8.36 Å, 0.00139, 5.17 g/cm³, 584.28 Å³, 1.11×10^{17} lines/m², and 30.37%, respectively. The results were close to that of reported for other ferrites such as Mg-substituted ZnFe₂O₄, MgFe₂O₄, and ZnFe₂O₄. However, the results were closer to ZnFe₂O₄ system more than to MgFe₂O₄ owing to the presence of Zn²⁺ ion in the former.^{44–46}

3.2. Optical Analysis. The optical properties of the prepared cobalt copper zinc ferrite nanoparticles were determined using UV-vis spectroscopy. In the electromagnetic spectrum, ions, atoms, or molecules undergo electronic transitions from the ground to excited state or excitation of electrons from the valence band (oxides-2p orbital) to the conduction band (iron, Fe-3d orbital) released absorption

spectrum in the range of 200 nm –800 nm UV-vis light wavelength. The optical absorbance and energy band gap result was shown in Figure 2 panels (A) and (B), respectively. The broad spectrum of spinel ferrite CoCuZnFe₂O₄ nanoparticles was depicted and the absorbance peak found at ~300 nm wavelength indicates the presence of nanosized particles and the formation of ferrite. Moreover, the direct transition band gap energy was estimated from the intercept of $(\alpha h\nu)^2$ versus $h\nu$ using Tauc's relation^{47–49} and it can be influenced by the presence of impurities, and structural properties like particle size, lattice parameters, and many more.^{50–52} The Tauc's relation is

$$(\alpha h\nu)^2 = A(h\nu - E_g) \quad (4)$$

where Planck's constant (h) is 4.136×10^{-15} eV·sec, the velocity of light (c) is 3×10^{17} nm/sec, λ is absorbance wavelength, α is absorption coefficient, E_g is the energy band gap, and A is a proportionality constant. The plot of $(\alpha h\nu)^2$ against photon energy ($h\nu$) has a curvature line for which an extrapolated straight line to x -axis gives the value of the indirect optical energy gap (E_g).

Here, the band gap energy (E_g) of CoCuZnFe₂O₄ was 2.6 eV (Figure 2(B)). This revealed that electron density in the conduction band was increased; thus, its lower E_g value helps in the fast movement of electron transition during the thermal decomposition study of ammonium nitrate. The band gap energy was close to that reported by Jadhav et al. for NiFe₂O₄ 26.6 nm (2.59 eV)²⁴ and 14 nm (2.26 eV).²⁵

3.3. Molecular Polarization. Raman spectroscopy helps to determine structural changes in the chemical species due to polarization of molecules, and it depends on mass and bond strength of the molecule. If molecules have higher mass and a longer bond, Raman peaks shift to the higher wavenumbers (red shift) and vice versa. In this study, we have monitored the effect of the synthesized nanocatalyst cobalt copper zinc ferrite (CoCuZnFe₂O₄) on the Raman spectrum of ammonium nitrate. Their Raman spectra were displayed in Figure 3.

Spinel ferrite CoCuZnFe₂O₄ has octahedral and tetrahedral sites in which A_{1g} , E_g , and $3T_{2g}$ are Raman active modes that are responsible for molecular vibrations. Bands were found in the range of 200 cm⁻¹–1200 cm⁻¹ Raman shift. The bending vibration of the metal–oxygen bond occurred at the octahedral site < 650 cm⁻¹, and the symmetric stretching vibration of the metal–oxygen bond occurred at the tetrahedral site > 650 cm⁻¹. In these sites, A_{1g} and E_g molecular vibrations occurred between 450 cm⁻¹ and 630 cm⁻¹ Raman shift, while $3T_{2g}$

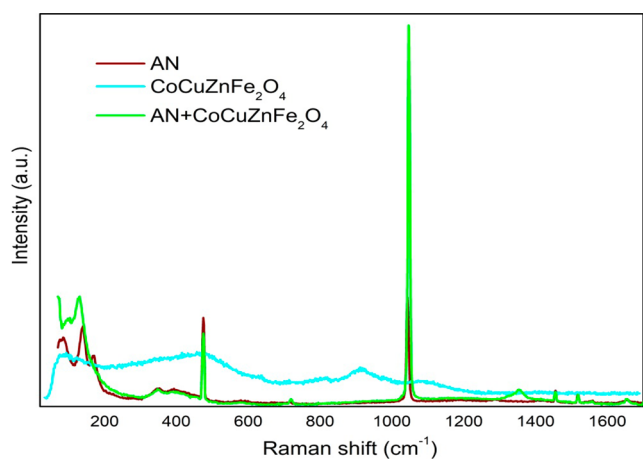


Figure 3. Comparative Raman spectra of AN, CoCuZnFe₂O₄, and AN + CoCuZnFe₂O₄.

molecular vibration occurred between 700 cm⁻¹ and 1000 cm⁻¹ Raman shift (Figure 3). Moreover, a lower region Raman shift was found due to translation movement of the metal–oxygen bond at the tetrahedral site.^{53,54}

Ammonium nitrate (AN) has Raman active modes in the range 50 cm⁻¹ to 1600 cm⁻¹ in which a lower frequency mode (<200 cm⁻¹) was assigned to crystallographic transformation of enantiotropic phases of AN while moderate frequency modes (250 cm⁻¹ to 800 cm⁻¹) were assigned to molecular vibrations of orientation disorder of cations and anions of N–O bond of nitrate group (NO₃⁻) and higher frequency modes (<800 cm⁻¹) were assigned to heteroionic coupling effect of ammonium ion (NH₄⁺) and nitrate ion (NO₃⁻). The intense peaks observed at ~480 cm⁻¹ Raman shift correspond to N–O and N–H bending vibrations, while the characteristic peak of AN at ~1050 cm⁻¹ Raman shift corresponds to NO₃⁻ symmetric vibration.^{55–57} It was observed that at room temperature and ambient pressure in the presence of a nanocatalyst ternary spinel ferrite CoCuZnFe₂O₄ shifted bands as observed due to molecular bonding polarization with ammonium nitrate, which resulted in increasing the characteristic peak intensity of AN. However, the blue shift in AN + CoCuZnFe₂O₄ observed indicates the size effect of nanoferrite. Moreover, the increment of smaller bands in the region of 1300 cm⁻¹ to 1600 cm⁻¹ was assigned to specific interaction of the heteromolecular deformation of NH₄⁺ and NO₃⁻ due to presence of nanosized CoCuZnFe₂O₄.

3.4. Morphology. The morphology of ammonium nitrate (AN) and CoCuZnFe₂O₄ was shown in Figure 4-A and Figure 4-B, respectively. The SEM micrographs of AN showed a rough surface looking like a honeycomb structure while CoCuZnFe₂O₄ nanoparticles have a polyhedron shape with

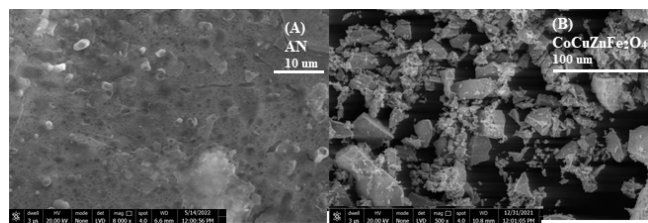


Figure 4. FE-SEM images of (A) AN and (B) nanocatalyst CoCuZnFe₂O₄.

some agglomerations. The average particle size of CoCuZnFe₂O₄ was calculated using ImageJ software and it was ~11 nm.

3.5. TG-DSC Analysis. The thermal decomposition analysis of spinel ferrite CoCuZnFe₂O₄ was shown in Figure 5. Tritransition metal ferrite has endothermic gravimetric thermal decomposition with a weight loss of ~20% (Figure 5(A)). This result was also correlated with DSC analysis (Figure 5(B)). Decomposition steps included desorption of water molecules (<150 °C) having an exothermic phase, and the presence of organic impurities or formation of metal oxides (200 to 700 °C) has an endothermic phase. This synthesized nanocatalyst CoCuZnFe₂O₄ showed thermal stability with the least weight loss.

3.6. Thermal Decomposition of AN without Nanocatalyst. Figure 6 depicts the typical DSC curve for pure ammonium nitrate over the temperature range from 50 to 420 °C and atmospheric pressure, within which few thermal steps are observed. In this curve, five endothermic peaks were produced in the heating process of AN. Due to enantiotropic phase changes from orthorhombic to tetragonal and tetragonal to cubic, the first three distinct broad peaks are found at 60 °C, 90 °C, and 127 °C, respectively. The melting point of AN was assigned to the fourth endothermic peak, which was discovered at 170 °C. After this phase, the decomposition of liquid AN starts and results in gaseous products. The intense decomposition peak of ammonium nitrate at 298 °C was assigned the fifth endothermic phase. In an open system, gaseous products like NH₃, HNO₃, N₂O, and H₂O are created during the thermal breakdown of ammonium nitrate. These gaseous products can only be the chemical gases that are evacuated and quickly cooled. Thus, the decomposition process is seen to be endothermic.^{57,58}

3.7. Thermal Decomposition of AN with Nanocatalyst CoCuZnFe₂O₄. The effect of nanocatalyst CoCuZnFe₂O₄ on the DSC curve of ammonium nitrate (AN) thermal decomposition was studied in a nitrogen atmosphere, and it was observed that the CoCuZnFe₂O₄ spinel ferrite has a significant effect on the rate of AN decomposition, as shown in Figure 7. Furthermore, as the heating rate of AN+CoCuZnFe₂O₄ changed from 5, 10, and 15 °C/min during thermal treatment, the decomposition curve shifted to a higher temperature.

The DSC curve of AN+CoCuZnFe₂O₄ exhibits endothermic peaks throughout thermal treatment that correspond to the transformation of orthorhombic AN to tetragonal AN to cubic AN, melting of AN, and decomposition of AN. This mechanism of AN thermal decomposition into gaseous products has received a lot of attention in the literature.^{56–61} The complete decomposition of AN (NH₄NO₃) results in gaseous products such as N₂O, NO, NO₂, H₂O, and N₂. In the presence of nanocatalyst CoCuZnFe₂O₄ improved electron transformation of O₂ to O²⁻ during NH₄NO₃ decomposition or proton transfer reaction, which leads to the formation of ammonia and nitric acid from the vaporized ammonium nitrate, which can be further decomposed to HNO₃ and NH₃, and finally it helps in the subsequent oxidation of NH₃ that produces gaseous products. Moreover, the presence of CoCuZnFe₂O₄ shifted the endothermic peaks to lower temperatures (Figure 7) and it decreased the thermal decomposition temperature peak of AN by 25 °C, which showed its significant catalytic activity for lowering the thermal decomposition temperature of ammonium nitrate. The

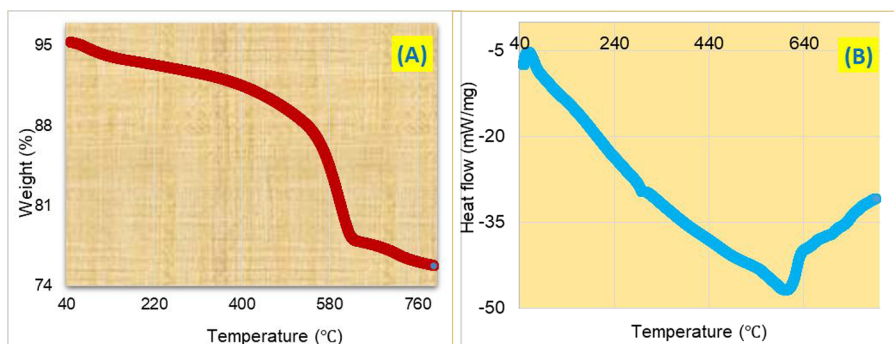


Figure 5. Thermographs of $\text{CoCuZnFe}_2\text{O}_4$ (A) TG and (B) DSC analysis.

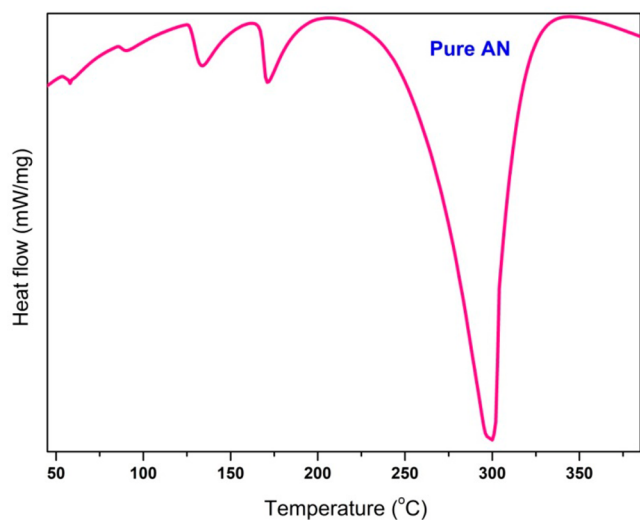


Figure 6. DSC thermograph of pure AN without catalyst.

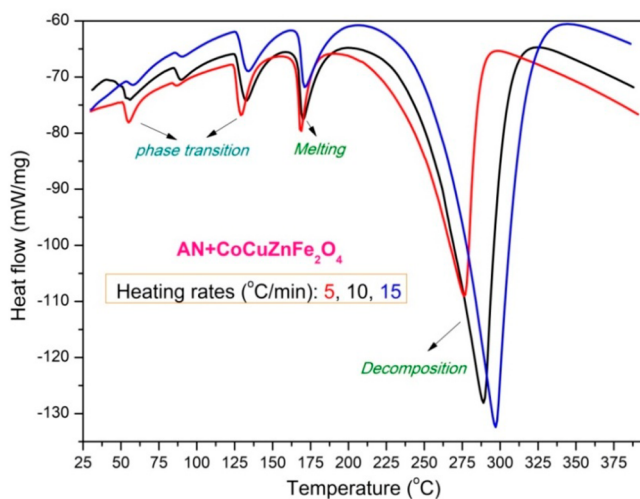


Figure 7. DSC thermograph of AN in the presence of nanocatalyst $\text{CoCuZnFe}_2\text{O}_4$ at 5, 10, and 15 °C/min.

catalytic activity of $\text{CoCuZnFe}_2\text{O}_4$ was further confirmed by the decreased activation energy of ammonium nitrate in the presence of a $\text{CoCuZnFe}_2\text{O}_4$ spinel ferrite nanocatalyst. The Arrhenius relation was used for the calculation of the activation energy of ammonium nitrate in the presence of nanocatalyst $\text{CoCuZnFe}_2\text{O}_4$. The DSC kinetics study was carried out at three different heating rates (5, 10, and 15 °C/min).

Moreover, thermal behavior of $\text{AN}+\text{CoCuZnFe}_2\text{O}_4$ was further explained by DTA-TG experiment. Figure 8 and 9

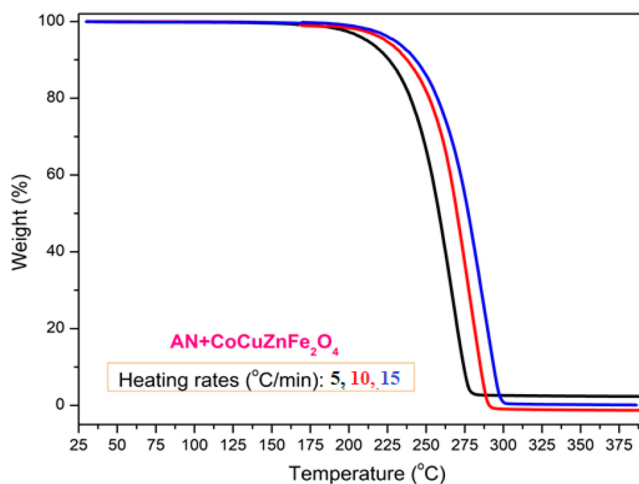


Figure 8. TG thermograph of AN in the presence of nanocatalyst $\text{CoCuZnFe}_2\text{O}_4$ at 5, 10, and 15 °C/min.

show TG-DTA curves of AN in the presence of nanocatalyst $\text{CoCuZnFe}_2\text{O}_4$ in inert nitrogen atmosphere with 5, 10, and 15 °C/min heating rates. One important peak in DTA thermograph and one decomposition step in the TG thermograph were observed. The TG thermograph revealed single stage decomposition started after the melting point of AN (~170 °C), and it was obvious that the decomposition temperature has a tiny variation with increasing the rate of heating. Total weight loss observed between 97% to 99%, indicate that AN decomposition was totally completed during the process of thermolysis.

However, additional information from DTA analysis has been incorporated to investigate the effects of analysis parameters like electromotive force and temperature difference on the thermal decomposition of AN with nanocatalyst $\text{CoCuZnFe}_2\text{O}_4$. The information obtained from DTA analysis was similar to that obtained from DSC analysis, but the only difference was in the curve patterns that changed from unit Watt to microvolt or Celsius, per milligram sample. The differential thermal analysis (DTA) thermograph of $\text{AN}+\text{CoCuZnFe}_2\text{O}_4$ was represented in Figure 9, in which (A) displayed the thermolysis of AN with nanocatalyst $\text{CoCuZnFe}_2\text{O}_4$ in terms of electromotive force difference while (B) displayed thermolysis values in terms of temperature differences. In both cases, as heating rate increased, peak intensity

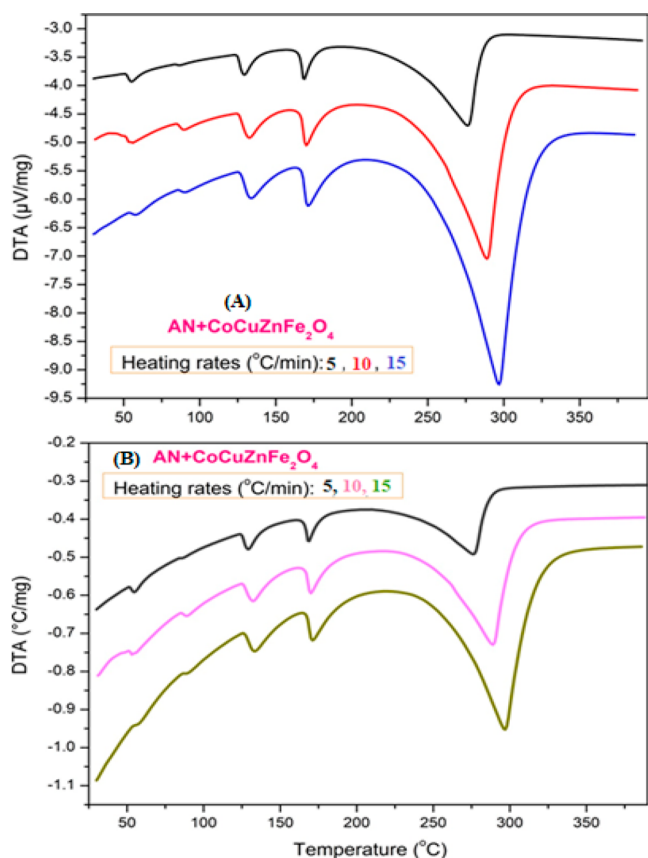


Figure 9. DTA thermograph of AN in the presence of nanocatalyst CoCuZnFe₂O₄ at 5, 10, and 15 °C/min (A) in $\mu\text{V}/\text{mg}$ unit and (B) in $^{\circ}\text{C}/\text{mg}$ unit.

increased, and the curve shifted to higher values of V/mg or $^{\circ}\text{C}/\text{mg}$ (y-axis) and, similarly, as the temperature of heating increased, peaks shifted toward higher temperatures (x-axis). The five endothermic phases observed have similar characteristics as those discussed previously in the DSC thermograph of AN. However, in the DTA curve, the first two endothermic phase transition peaks appeared widened. This may have occurred because of less difference in potential during thermal treatment.

3.8. Thermo-Kinetic Approach. Thermo-kinetic parameters, mainly activation energy and Gibbs free energy of activation, were calculated using the following relation of heating rate and decomposition peak temperature.

$$k = A \exp\left(-\frac{E}{RT_p}\right) \quad (5)$$

$$k = \frac{K_B T_B}{h} \exp\left(\frac{-\Delta G^\ddagger}{RT_p}\right) \quad (6)$$

$$\ln \frac{\beta}{T_p^2} = \ln \frac{R_A}{E} - \frac{E}{RT_p} \quad (7)$$

In these equations, T_p = decomposition peak temperature, k = rate of reaction, A = constant that depends on the presence of types of chemicals, E = the activation energy, K_B = Boltzmann constant (1.381×10^{-23} J/K), and h = Plank constant (6.626×10^{-34} J-s), R = universal gas constant (0.008314 kJ/K-mol), β = heating rate of thermal treatment, and ΔG^\ddagger = the activation

Gibbs free energy. The slope and intercept from the line plot of $\ln(\beta/T_p^2)$ against $1/T_p$ are used to obtain the activation energy and pre-exponential factor, respectively. Pure AN activation energy without catalyst was ~ 158 kJ/mol and AN with nanocatalyst CoCuZnFe₂O₄ was ~ 108 kJ/mol (Figure 10). This is a significant result because decomposition of AN

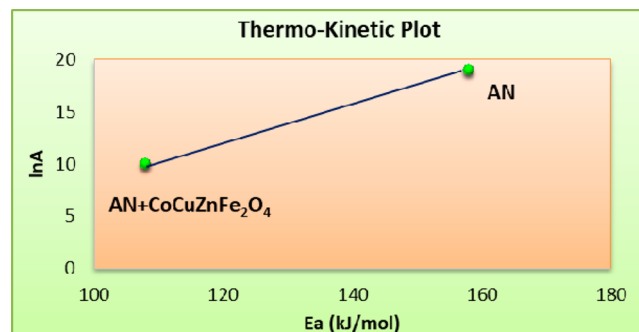
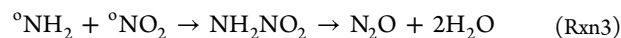
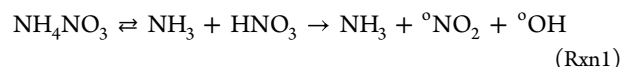


Figure 10. Thermo-kinetic plot of AN with and without nano-CoCuZnFe₂O₄.

in the presence of nano-CoCuZnFe₂O₄ should be initiated more quickly than the decomposition of pure AN. ΔG^\ddagger had positive values for pure AN (~ 129 kJ/mol) and for AN + CoCuZnFe₂O₄ (~ 91 kJ/mol), which means that the decomposition of AN will not be initiated spontaneously.

3.9. Plausible Mechanism of Thermal Decomposition of AN. According to the literature⁶² AN can decompose according to reactions Rxn1–Rxn3 at high temperatures. Ferrites at high temperatures can yield $^{\circ}\text{OH}$ which may facilitate the decomposition, and as well, metal ions may adsorb the gas released during the decomposition. NH₃ can be oxidized by holes and HO• breaking the original NH₃ metal ferrite adsorption equilibrium facilitating Rxn1–Rxn3.



4. CONCLUSIONS

The coprecipitation method can be effectively used for the synthesis of 9–22 nm size particles of CoCuZnFe₂O₄ with a low optical band gap of 2.6 eV. The low band gap and nanosize of CoCuZnFe₂O₄ can facilitate the decomposition temperature and kinetics of AN, which can directly influence the burning rate of AN based solid propellants. In the presence of CoCuZnFe₂O₄, the major thermal decomposition peak temperature of AN was decreased by 27 °C with a mass loss ~ 97 –99% suggesting completely decomposition of AN. The activation energy of AN decreased from 158 to 108 kJ/mol in the presence of CoCuZnFe₂O₄, confirming its catalytic activity. The lower value of $\ln A$ suggests faster thermal decomposition of AN in the presence of catalyst compared to that of pure AN, which could be used to provide thrust to an object within a short span of time. The AN + 2 wt % CoCuZnFe₂O₄ composition can be used in solid rocket propellants as a greener energetic composition compared to ammonium perchlorate-based propellants.

■ ASSOCIATED CONTENT

SI Supporting Information

The Supporting Information is available free of charge at <https://pubs.acs.org/doi/10.1021/acsomega.2c04796>.

Figure S1. XRD pattern list of CoCuZnFe₂O₄ compared with ref. no. 01-077-0012 and Table S1. BET surface area analysis data CoCuZnFe₂O₄ (Autosorb iQ Station 2 using nitrogen gas as absorbate in 12 mm w/o rod type cell) (PDF)

■ AUTHOR INFORMATION

Corresponding Author

Pragnesh N Dave – Department of Chemistry, Sardar Patel University, Vallabh Vidyanagar 388 120 Gujarat, India;
orcid.org/0000-0002-8817-208X; Email: pragnesh7@yahoo.com

Author

Ruksana Sirach – Department of Chemistry, Sardar Patel University, Vallabh Vidyanagar 388 120 Gujarat, India

Complete contact information is available at:

<https://pubs.acs.org/10.1021/acsomega.2c04796>

Notes

The authors declare no competing financial interest.

■ ACKNOWLEDGMENTS

The authors are grateful to Department of Chemistry and Department of Physics, Sardar Patel University for providing research facility and instrumental facility and Savitribai Phule Pune University for providing TG-DSC facility. RS is thankful to Department of Science and Technology (DST), New Delhi, India for providing financial support from grant number SR/NM/NT-1014/2016 (G) for Junior Research fellowship, respectively. The authors are thankful to Charutar Vidya Mandal (CVM) University, Gujarat, India for the FEG-SEM facility.

■ REFERENCES

- (1) Wang, Y.; Song, X.; Li, F. Thermal Behavior and Decomposition Mechanism of Ammonium Perchlorate and Ammonium Nitrate in the Presence of Nanometer Triaminoguanidine Nitrate. *ACS Omega* **2019**, *4*, 214–225.
- (2) Lysien, K.; Stolarczyk, A.; Jarosz, T. Solid Propellant Formulations: A Review of Recent Progress and Utilized Components. *Materials (Basel)* **2021**, *14*, 6657.
- (3) Sovizi, M. R.; Hajimirsadeghi, S. S.; Naderizadeh, B. Effect of Particle Size on Thermal Decomposition of Nitrocellulose. *J. Hazard. Mater.* **2009**, *168*, 1134–1139.
- (4) Rubtsov, Y. I.; Kazakov, A. I.; Lempert, D. B.; Manelis, G. B. Kinetics and Mechanism of Thermal Decomposition of Guanidinium Nitrate and Its Mixtures with Ammonium Nitrate. *Russ. J. Appl. Chem.* **2004**, *77*, 1083–1091.
- (5) Kumar, M.; Singh Dosanjh, H.; Sonika, Singh, J.; Monir, K.; Singh, H. Review on Magnetic Nanoferrites and Their Composites as Alternatives in Waste Water Treatment: Synthesis, Modifications and Applications. *Environ. Sci. Water Res. Technol.* **2020**, *6*, 491–514.
- (6) Singh, S.; Sahai, A.; Katyal, S. C.; Goswami, N. Structural, Optical and Vibrational Study of Zinc Copper Ferrite Nanocomposite Prepared by Exploding Wire Technique. *Mater. Sci. Polym.* **2018**, *36*, 722–732.
- (7) Swiderski, G. S.; Wilczewska, a. Z.; Swislocka, R.; Kalinowska, M.; Lewandowski, W. Spectroscopic (IR, Raman, UV-Vis) Study and

Thermal Analysis of 3d-Metal Complexes with 4-Imidazolecarboxylic Acid. *J. Therm. Anal. Calorim.* **2018**, *134*, 513–525.

(8) Yang, M.; Chen, X.; Wang, Y.; Yuan, B.; Niu, Y.; Zhang, Y.; Liao, R.; Zhang, Z. Comparative Evaluation of Thermal Decomposition Behavior and Thermal Stability of Powdered Ammonium Nitrate under Different Atmosphere Conditions. *J. Hazard. Mater.* **2017**, *337*, 10–19.

(9) Lurie, B. A.; Lianshen, C. Kinetics and Mechanism of Thermal Decomposition of Ammonium Nitrate Powder under the Action of Carbon Black. *Combust. Explos. Shock Waves.* **2000**, *36*, 607–617.

(10) Yang, M.; Chen, X.; Yuan, B.; Wang, Y.; Rangwala, A. S.; Cao, H.; Niu, Y.; Zhang, Y.; Fan, A.; Yin, S. Inhibition Effect of Ammonium Dihydrogen Phosphate on the Thermal Decomposition Characteristics and Thermal Sensitivity of Ammonium Nitrate. *J. Anal. Appl. Pyrolysis* **2018**, *134*, 195–201.

(11) Gunawan, R.; Zhang, D. Thermal Stability and Kinetics of Decomposition of Ammonium Nitrate in the Presence of Pyrite. *J. Hazard. Mater.* **2009**, *165*, 751–758.

(12) Izato, Y. i.; Shiota, K.; Miyake, A. Condensed-Phase Pyrolysis Mechanism of Ammonium Nitrate Based on Detailed Kinetic Model. *J. Anal. Appl. Pyrolysis* **2019**, *143*, 143.

(13) Kaniowski, M.; Hoffmann, K.; Hoffmann, J. Influence of Selected Potassium Salts on Thermal Stability of Ammonium Nitrate. *Thermochim. Acta* **2019**, *678*, 178313.

(14) Oluwoye, I.; Mosallanejad, S.; Soubans, G.; Altarawneh, M.; Gore, J.; Dlugogorski, B. Z. Thermal Decomposition of Ammonium Nitrate on Rust Surface: Risk of Low-Temperature Fire. *Fire Saf. J.* **2021**, *120*, 103063.

(15) EL-Sayed, S. A. Review of Thermal Decomposition, Kinetics Parameters and Evolved Gases during Pyrolysis of Energetic Materials Using Different Techniques. *J. Anal. Appl. Pyrolysis* **2022**, *161*, 105364.

(16) Wang, X.; Pei, C.; Wu, X.; Xu, F.; Yang, N.; Liu, D.; Xu, S. Experiment-Based Cause Analysis of Secondary Explosion of Ammonium Nitrate in Fire Conditions. *J. Loss Prev. Process Ind.* **2022**, *77*, 104780.

(17) Mukherjee, D.; Sen, N.; Singh, K. K.; Saha, S.; Shenoy, K. T.; Marathe, P. P. Real Time Concentration Estimation of Ammonium Nitrate in Thermal Denitration Process: An Ultrasonic Approach. *Sensors Actuators A Phys.* **2021**, *331*, 112927.

(18) Izato, Y.-I.; Miyake, A. Thermal Decomposition of Molten Ammonium Nitrate (AN) Chemical Equilibrium in Molten AN. *J. Therm. Anal. Calorim.* **2015**, *122*, 595–600.

(19) Skarlis, S. A.; Nicolle, A.; Berthout, D.; Dujardin, C.; Granger, P. Combined Experimental and Kinetic Modeling Approaches of Ammonium Nitrate Thermal Decomposition. *Thermochim. Acta* **2014**, *584*, 58–66.

(20) Gilani, Z. A.; Shifa, M. S.; Chandio, A. D.; Usmani, M. N.; Aslam, S.; Khalid, M.; Perveen, A.; Rehman, J. U. R.; Mustaqeem, M.; Khan, M. A.; Sciences, M. Thermogravimetric Analysis, Optical And Dielectric Properties Of Newly Developed LiNi_{0.3}Pr_xFe_{2-x}O₄ Nanocrystalline Ferrites. *J. Nanomater. Biostruct.* **2018**, *13*, 809–816.

(21) Ladole, C. A. Preparation And Characterization Of Spinel Zinc Ferrite ZnFe₂O₄. *Int. J. Chem. Sci.* **2012**, *10*, 1230–1234.

(22) Kumar, M.; Singh Dosanjh, H.; Sonika Singh, J.; Monir, K.; Singh, H. Review on Magnetic Nanoferrites and Their Composites as Alternatives in Waste Water Treatment: Synthesis, Modifications and Applications. *Environ. Sci. Water Res. Technol.* **2020**, *6*, 491–514.

(23) Elbasuney, S.; Yehia, M. Ferric Oxide Colloid : A Novel Nano - Catalyst for Solid Propellants. *J. Inorg. Organomet. Polym. Mater.* **2020**, *30*, 706–713.

(24) Jadhav, S. A.; Raut, A. V.; Khedkar, M. V.; Somvanshi, S. B.; Jadhav, K. M. Photocatalytic Activity of Nickel Ferrite Nanoparticles Synthesized via Sol-Gel Auto Combustion Method. *Advanced Materials Research.* **2022**, *1169*, 123–127.

(25) Jadhav, S. A.; Khedkar, M. V.; Somvanshi, S. B.; Jadhav, K. M. Magnetically retrievable nanoscale nickel ferrites: an active photocatalyst for toxic dye removal applications. *Ceram. Int.* **2021**, *47* (20), 28623–28633.

- (26) Borade, R. M.; Somvanshi, S. B.; Kale, S. B.; Pawar, R. P.; Jadhav, K. M. Spinel zinc ferrite nanoparticles: an active nanocatalyst for microwave irradiated solvent free synthesis of chalcones. *Materials Research Express* **2020**, *7* (1), 016116.
- (27) Somvanshi, S. B.; Kharat, P. B.; Jadhav, K. M. Surface Functionalized Superparamagnetic Zn-Mg Ferrite Nanoparticles for Magnetic Hyperthermia Application Towards Noninvasive Cancer Treatment. *Macromol. Symp.* **2021**, *400* (1), 2100124.
- (28) Kharat, P. B.; Somvanshi, S. B.; Somvanshi, S. B.; Mopari, A. M. Low-cost Fabrication of Zn-doped MnFe₂O₄ (Mn_{0.5}Zn_{0.5}Fe₂O₄) Film for H₂S Gas Sensing Applications. *Macromol. Symp.* **2021**, *400* (1), 2100147.
- (29) Ion, R.; Toma, L. G. Analytical Studies of Ferrite Nanoparticles. *J. Optoelectron. Adv. Mater.* **2010**, *12*, 2113–2118.
- (30) Chand, P.; Vaish, S.; Kumar, P. Structural, Optical and Dielectric Properties of Transition Metal (MFe₂O₄; M = Co, Ni and Zn) Nanoferrites Structural, Optical and Dielectric Properties of Transition Metal (MFe₂O₄; M = Co, Ni and Zn) Nanoferrites. *Phys. B Phys. Condens. Matter* **2017**, *524*, 53–63.
- (31) Zhang, H.; Zhou, Y.; Liu, S.-Q.; Gu, Q.-Q.; Meng, Z.-D.; Luo, L. Molecular-Level Understanding of Selectively Photocatalytic Degradation of Ammonia via Copper Ferrite/N-Doped Graphene Catalyst under Visible Near-Infrared Irradiation. *Catalysts* **2018**, *8*, 405.
- (32) Chavan, A. R.; Khirade, P. P.; Somvanshi, S. B.; Mukhamale, S. V.; Jadhav, K. M. Eco-friendly green synthesis and characterizations of CoFe_{2-x}Al_xO₄ nanocrystals: analysis of structural, magnetic, electrical, and dielectric properties. *Journal of Nanostructure in Chemistry* **2021**, *11* (3), 469–481.
- (33) Khirade, P. P.; Chavan, A. R.; Somvanshi, S. B.; Kounsalye, J. S.; Jadhav, K. M. Tuning of physical properties of multifunctional Mg-Zn spinel ferrite nanocrystals: a comparative investigations manufactured via conventional ceramic versus green approach sol-gel combustion route. *Materials Research Express* **2020**, *7* (11), 116102.
- (34) Humbe, A. V.; Somvanshi, S. B.; Kounsalye, J. S.; Kumar, A.; Jadhav, K. M. Influential trivalent ion (Cr³⁺) substitution in mixed Ni-Zn nanoferrites: Cation distribution, magnetic, Mossbauer, electric, and dielectric studies. *Ceram. Int.* **2022**, *48*, 34075.
- (35) Vinosha, P. A.; Mely, L. A.; Mary, G. I. N.; Mahalakshmi, K.; Vinosha, P. A.; Mely, L. A.; Mary, G. I. N.; Mahalakshmi, K.; Das, S. J. Study on Cobalt Ferrite Nanoparticles Synthesized by Co-Precipitation Technique for Photo-Fenton Application. *Mech., Mater. Sci. Eng. J.* **2017**, 0–6.
- (36) Dave, P.; Sirach, R.; Thakkar, R.; Deshpande, M. P.; Badgujar, D. M. Cobalt copper zinc ferrite: An efficient catalyst for the thermal decomposition of ammonium perchlorate. *Combust. Sci. Technol.* **2022**, 1–18.
- (37) Mushtaq, M. W.; Imran, M.; Bashir, S.; Kanwal, F.; Mitu, L. Synthesis, Structural and Biological Studies of Cobalt Ferrite Nanoparticles. *Mater. Sci., Chem.* **2016**, *48*, 565–570.
- (38) Šutka, A.; Pärna, R.; Kleperis, J.; Käämbre, T.; Pavlovskaja, I.; Korsaks, V.; Malnieks, K.; Grinberga, L.; Kisand, V. Photocatalytic activity of non-stoichiometric ZnFe₂O₄ under visible light irradiation. *Phys. Scr.* **2014**, *89*, 044011.
- (39) Shaikh, S. F.; Ubaidullah, M.; Mane, R. S. Types, Synthesis Methods and Applications of Ferrites. *Spinel Ferrite Nanostructures for Energy Storage Devices* **2020**, 51–81, DOI: 10.1016/B978-0-12-819237-5.00004-3.
- (40) Fountain, A. W.; Christesen, S. D.; Moon, R. P.; Guicheteau, J. A.; Emmons, E. D. Recent Advances and Remaining Challenges for the Spectroscopic Detection of Explosive Threats. *Appl. Spectrosc.* **2014**, *68*, 795–811.
- (41) Dippong, T.; Levei, E.-A.; Lengauer, C. L.; Daniel, A.; Toloman, D.; Cadar, O. Materials Characterization Investigation of Thermal, Structural, Morphological and Photocatalytic Properties of Cu_xCo_{1-x}Fe₂O₄ (0 ≤ x ≤ 1) Nanoparticles Embedded in SiO₂ Matrix. *Mater. Charact.* **2020**, *163*, 110268.
- (42) Bhatt, S. V.; Deshpande, M. P.; Sathe, V.; Rao, R.; Chaki, S. H. Raman Spectroscopic Investigations on Transition-Metal Dichalcogenides MX₂ (M = Mo, W; X = S, Se) at High Pressures and Low Temperature. *J. Raman Spectrosc.* **2014**, *45*, 971–979.
- (43) Trache, D. *Materials Horizons: From Nature to Nanomaterials*; Springer, 2019; DOI: 10.1007/978-981-15-9223-2.
- (44) Somvanshi, S. B.; Kharat, P. B.; Khedkar, M. V.; Jadhav, K. M. Hydrophobic to hydrophilic surface transformation of nano-scale zinc ferrite via oleic acid coating: magnetic hyperthermia study towards biomedical applications. *Ceram. Int.* **2020**, *46* (6), 7642–7653.
- (45) Somvanshi, S. B.; Khedkar, M. V.; Kharat, P. B.; Jadhav, K. M. Influential diamagnetic magnesium (Mg²⁺) ion substitution in nano-spinel zinc ferrite (ZnFe₂O₄): thermal, structural, spectral, optical and physisorption analysis. *Ceram. Int.* **2020**, *46* (7), 8640–8650.
- (46) Somvanshi, S. B.; Patade, S. R.; Andhare, D. D.; Jadhav, S. A.; Khedkar, M. V.; Kharat, P. B.; Khirade, P. P.; Jadhav, K. M. Hyperthermic evaluation of oleic acid coated nano-spinel magnesium ferrite: enhancement via hydrophobic-to-hydrophilic surface transformation. *J. Alloys Compd.* **2020**, *835*, 155422.
- (47) Khan, S. B.; Irfan, S.; Lee, S.-L. Influence of Zn + 2 Doping on Ni-Based Nanoferrites. *Nanomaterials* **2019**, *9*, 1024.
- (48) Velinov, N.; Petrova, T.; Ivanova, R.; Tsoncheva, T.; Kovacheva, D.; Mitov, I. Synthesis and Characterization of Copper-Nickel Ferrite Catalysts for Ethyl Acetate Oxidation. *Hyperfine Interact.* **2020**, *241*, 1–12.
- (49) Wu, Q.; Tan, L.; Xu, S.; Liu, D.; Min, L. Study on Thermal Decomposition Characteristics of Ammonium Nitrate Emulsion Explosive in Different Scales. *J. Energy Mater.* **2018**, *36*, 202–210.
- (50) Xu, Z.-X.; Cheng, J.-H.; Wang, Q.; Cheng, J.; Hu, X. The Influence of Dissociation Reaction on Ammonium Nitrate Thermal Decomposition Reaction. *J. Therm. Anal. Calorim.* **2019**, *136*, 1415–1424.
- (51) Izato, Y.-i.; Miyake, A. Kinetic Analysis of the Thermal Decomposition of Liquid Ammonium Nitrate Based on Thermal Analysis and Detailed Reaction Simulations. *J. Therm. Anal. Calorim.* **2018**, *134*, 813–823.
- (52) Xu, Z.-X.; Xu, G.-S.; Fu, X.-Q.; Wang, Q. The Mechanism of Nano-CuO and CuFe₂O₄ Catalyzed Thermal Decomposition of Ammonium Nitrate. *Nanomater. Nanotechnol.* **2016**, *6*, 1–10.
- (53) Yang, M.; Chen, X.; Wang, Y.; Yuan, B.; Niu, Y.; Zhang, Y.; Liao, R.; Zhang, Z. Comparative Evaluation of Thermal Decomposition Behavior and Thermal Stability of Powdered Ammonium Nitrate under Different Atmosphere Conditions. *J. Hazard. Mater.* **2017**, *337*, 10–19.
- (54) Vargeese, A. A.; Muralidharan, K.; Krishnamurthy, V. N. Kinetics of Nano Titanium Dioxide Catalyzed Thermal Decomposition of Ammonium Nitrate and Ammonium Nitrate-Based Composite Solid Propellant. *Propellants Explos. Pyrotech.* **2015**, *40*, 260–266.
- (55) Akinin, N. I.; Vasin, A. Y.; Dubovik, A. V.; Anosova, E. B.; Gadzhiev, G. G.; Shushpanov, A. N.; Viktorov, S. D.; Frantov, A. E. Mechanical and Thermal Sensitivity of Mixtures of Ammonium Nitrate with Combustible Hydrocarbons. *Koks i Khimiya* **2018**, *61*, 40–44.
- (56) Asgari, A.; Ghani, K.; Keshavarz, M. H.; Mousaviyar, A.; Khajavian, R. Ammonium Nitrate-MOF-199: A New Approach for Phase Stabilization of Ammonium Nitrate. *Thermochim. Acta* **2018**, *667*, 148–152.
- (57) Oluwoye, I.; Altarawneh, M.; Gore, J.; Dlugogorski, B. Z. Burning Properties of Redox Crystals of Ammonium Nitrate and Saccharides. *Combust. Flame* **2020**, *213*, 132–139.
- (58) Cao, H. Q.; Duan, Q. L.; Chai, H.; Li, X. X.; Sun, J. H. Experimental Study of the Effect of Typical Halides on Pyrolysis of Ammonium Nitrate Using Model Reconstruction. *J. Hazard. Mater.* **2020**, *384*, 121297.
- (59) Yang, M.; Chen, X.; Yuan, B.; Wang, Y.; Rangwala, A. S.; Cao, H.; Niu, Y.; Zhang, Y.; Fan, A.; Yin, S. Inhibition Effect of Ammonium Dihydrogen Phosphate on the Thermal Decomposition Characteristics and Thermal Sensitivity of Ammonium Nitrate. *J. Anal. Appl.* **2018**, *134*, 195–201.

- (60) Ganesan, S.; Sridhar, B. Thermal Decomposition Characteristics of Ammonium Nitrate-Based Energetic Materials. *Int. J. Mech. Mechatronics* **2014**, *14*, 110–115.
- (61) EL-Sayed, S. A. Review of Thermal Decomposition, Kinetics Parameters and Evolved Gases during Pyrolysis of Energetic Materials Using Different Techniques. *J. Anal. Appl. Pyrolysis* **2022**, *161*, 105364.
- (62) Babrauskas, V.; Leggett, D. Thermal decomposition of ammonium nitrate. *Fire and Materials* **2020**, *44* (2), 250–268.